$[Zr_6O_4(OH)_4(benzene\text{-}1,4\text{-}dicarboxylato)_6]_n$: a hexagonal polymorph of UiO-66

Maite Perfecto-Irigaray, Garikoitz Beobide, Oscar Castillo, Ivan da Silva, Daniel García-Lojo, Antonio Luque, Ander Mendia and Sonia Pérez-Yáñez

Published version information

Citation: M Perfecto-Irigaray et al. "$[Zr_6O_4(OH)_4(benzene\text{-}1,4\text{-}dicarboxylato)_6]_n$: a hexagonal polymorph of UiO-66." Chemical Communications, vol. 55, no. 42 (2019): 5954-5957.

DOI: 10.1039/c9cc00802k

Journal Name

COMMUNICATION

$[Zr_6O_4(OH)_4(benzene\text{-}1,4\text{-}dicarboxylato)_6]_n$: a hexagonal polymorph of UiO-66

Received 00th January 20xx,
Accepted 00th January 20xx

DOI: 10.1039/x0xx00000x

www.rsc.org/

Maite Perfecto-Irigaray,[a] Garikoitz Beobide,*[a] Oscar Castillo,*[a] Ivan da Silva,[b] Daniel García-Lojo,[a] Antonio Luque,[a] Ander Mendia,[a] and Sonia Pérez-Yáñez [ac]

Since its discovery in 2008, the paradigmatic UiO-66 has behaved as the germ that has prompted the chemistry of group-4 metal based metal-organic frameworks, all of them featured by outstanding thermal and chemical stability. Herein we present the first polymorph of UiO-66 and key conditions that led to its formation.

MOFs (metal-organic frameworks) have evolved from being a field of study of a discreet part of the scientific community devoted to coordination chemistry, to supposing today an ubiquitous material in different areas.[1,2] Their great structural versatility have yielded an overwhelming number of inputs in the Cambridge Structural Database (CSD) which contains a subset for MOFs with more than 82,600 entries (i.e. a 9% of the CSD entries).[3,4] Most of published structures consist of divalent transition metal cations (Zn^{2+}, Cu^{2+}, Co^{2+}, Ni^{2+}, etc.). These MOFs are featured by poor chemical stability upon mild acid media, water or even humidity, which limit their applications. In order to overcome this limitation different approaches have been developed. One of them involves tuning ligand features, for instance, M(II)/azolates tend to be hydrothermally more stable than M(II)/carboxylates.[5] Another possibility relies on increasing the metal cation charge (together with its greater polarizing capability: charge/ionic radius) since it strengthens the metal-carboxylate bond and, therefore, the chemical stability.[6] The most successful case of this approach is represented by the metal ions of group 4 (Ti, Zr, Hf).[7] Their high oxidation state (4+) leads to stronger bonds and requires more ligands to balance the charge of the inorganic nodes, both factors contributing to prevent the chemical attack. As a result, MOFs of group 4 metals exhibit excellent stability in a broad range of solvents, water and even in extreme acid media. This improvement has supposed a breakthrough in the application of porous coordination polymers since the discovery in 2008 of the first Zr-MOFs consisting in the isoreticular series of UiO-66, -67 and -68.[8] The secondary building unit (SBU) of these structures, $[Zr_6(\mu_3\text{-}O)_4(\mu_3\text{-}OH)_4(\mu\text{-}COO)_{12}]$, is 12-fold connected by means of linear ditopic linkers (phenyl, biphenyl, and terphenyl, respectively) to yield a **fcu** type (face centered cubic) uninodal net. It must be emphasized that $[Zr_6(\mu_3\text{-}O)_4(\mu_3\text{-}OH)_4]^{12+}$ inorganic core is present in most of Zr-MOFs as it is readily formed under rather dissimilar synthesis conditions.[9] Consequently, the structural features of the inorganic node dominate the framework topology, and the strategy to obtain nets different to that of UiO-66 has consisted on replacing carboxylate groups of the linker by a pair of OH^-/H_2O to afford $[Zr_6(\mu_3\text{-}O)_4(\mu_3\text{-}OH)_4(OH)_x(OH_2)_x(\mu\text{-}COO)_{12-x}]$ 11-, 10-, 8-, and 6-connected clusters (x = 1, 2, 4, and 6, respectively).[10-13] Alternatively, the bridging polycarboxylates can be replaced by blocking monocarboxylates to further reduce the connectivity of the nodes.[14,15] In addition, other network topologies can be achieved by using other polytopic linkers. However, none of them can be considered strictly a polymorph of UiO-66, as the formulae differ.

Herein we present a new Zr-MOF, of formula $[Zr_6(\mu_3\text{-}O)_4(\mu_3\text{-}OH)_4(\mu_4\text{-}BDC)_6]_n$ (BDC: benzene-1,4-dicarboxylato) and named EHU-30 which was obtained through an alternative synthetic approach capable of modifying the framework topology retaining SBU and chemical formula of UiO-66: its first polymorphic form. Precisely, to synthesize EHU-30 the metal source (zirconium(IV) propoxide; 2.25 mmol; 70% wt in 1-propanol) was mixed under continuous stirring with methacrylic acid (8.17 mmol) and benzene-1,4-dicarboxylic acid (H_2BDC; 2.25 mmol). The resulting doughy reaction mixture was heated upon 140 °C for 90 minutes (see ESI). Thereafter, it was thoroughly washed with MeOH to obtain a white powder consisting on nanosized single-crystals of hexagonal prism

[a] Departamento de Química Inorgánica, Facultad de Ciencia y Tecnología, Universidad del País Vasco/Euskal Herriko Unibertsitatea, UPV/EHU, Apartado 644, E-48080 Bilbao, Spain.
[b] ISIS Facility, STFC Rutherford Appleton Laboratory, Chilton, Oxfordshire OX11 0QX, U.K.
[c] Departamento de Química Inorgánica, Facultad de Farmacia, Universidad del País Vasco/Euskal Herriko Unibertsitatea, UPV/EHU, E-01006 Vitoria-Gasteiz, Spain.

†Electronic Supplementary Information (ESI) available: synthesis and chemical characterization, synchrotron data collection and crystal structure elucidation, computational details and gas adsorption data. CCDC 1894173. For ESI and crystallographic data see DOI: 10.1039/x0xx00000x

Please do not adjust margins

shape (inset Fig. 1), which differ from the cubic habit featuring UiO-66 crystals. Fig. 1 compares the simulated powder X-ray diffraction pattern (PXRD) of UiO-66 with that of the new polymorph.

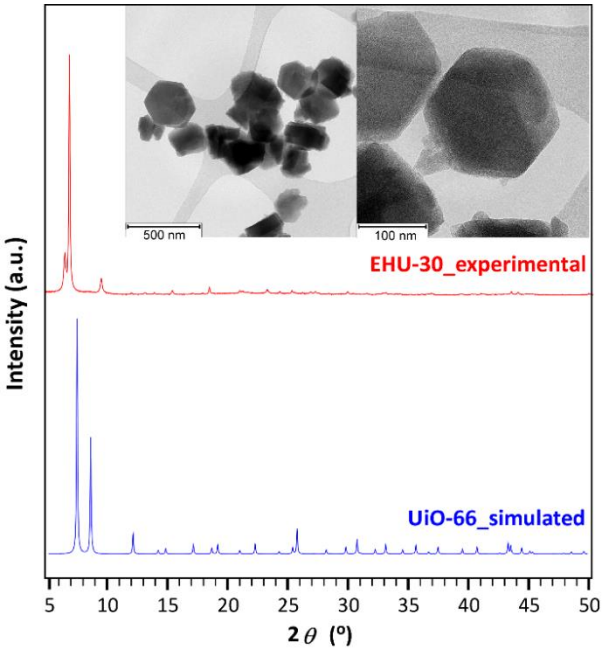

Fig 1. Experimental and simulated PXRD patterns for EHU-30 and UiO-66, respectively. Inset: TEM micrographs of EHU-30 nanosized crystals.

Note that previously reported synthesis of Zr-MOFs proceed under relatively diluted solvothermal conditions, using usually N,N-dimethylformamide as solvent.[16,17] On the contrary, EHU-30 is obtained under highly concentrated conditions, in which the modulator (methacrylic acid), apart from slowing down the nucleation and crystal growth,[18] exerts the template effect that directs the framework topology towards a kinetically favoured metastable structure (see discussion below). The hexagonal crystal structure of EHU-30 was determined *ab initio* from synchrotron X-ray powder diffraction data‡ (see ESI). The structural analysis shows how each $[Zr_6(\mu_3\text{-}O)_4(\mu_3\text{-}OH)_4(\mu\text{-}COO)_{12}]$ SBU is linked by means of twelve phenyl linkers to eight surrounding clusters, leading to an 8-connected uninodal three-dimensional net with hexagonal primitive topology (**hex**) and $(3^6{\cdot}4^{18}{\cdot}5^3{\cdot}6)$ point symbol,[19,20] while in UiO-66 each SBU is 12-connected into a **fcu**-type net. However, both polymorphs show a similar bidimensional hexagonal subnet (**hxl**) in which six of the BDC ligands are linking six coplanar Zr-SBUs (Fig. 2a), and therefore the structural difference arises from the assembly of these layers (Fig. S3.1 and S3.2). Accordingly, in UiO-66 each SBU is connected to three nodes of the upper layer and to another three of the lower layer, while in EHU-30 the SBU is linked to one each upper and lower layer SBUs by means of triple BDC pillars (Fig. 2b). An additional feature of EHU-30 lies on a rather unusual distortion observed for the BDC ligands comprising the triple pillar in which the carboxylate carbon atom lies out of the phenyl ring plane. This feature has been also observed in MOF-808 (M^{IV}: Zr, Hf).[15,21] The structural strain and the strength of the $Zr–O_{carboxylate}$ bond might be responsible for such distortion, but it must be taken with certain caution as the data arise from a PXRD Rietveld fitting.

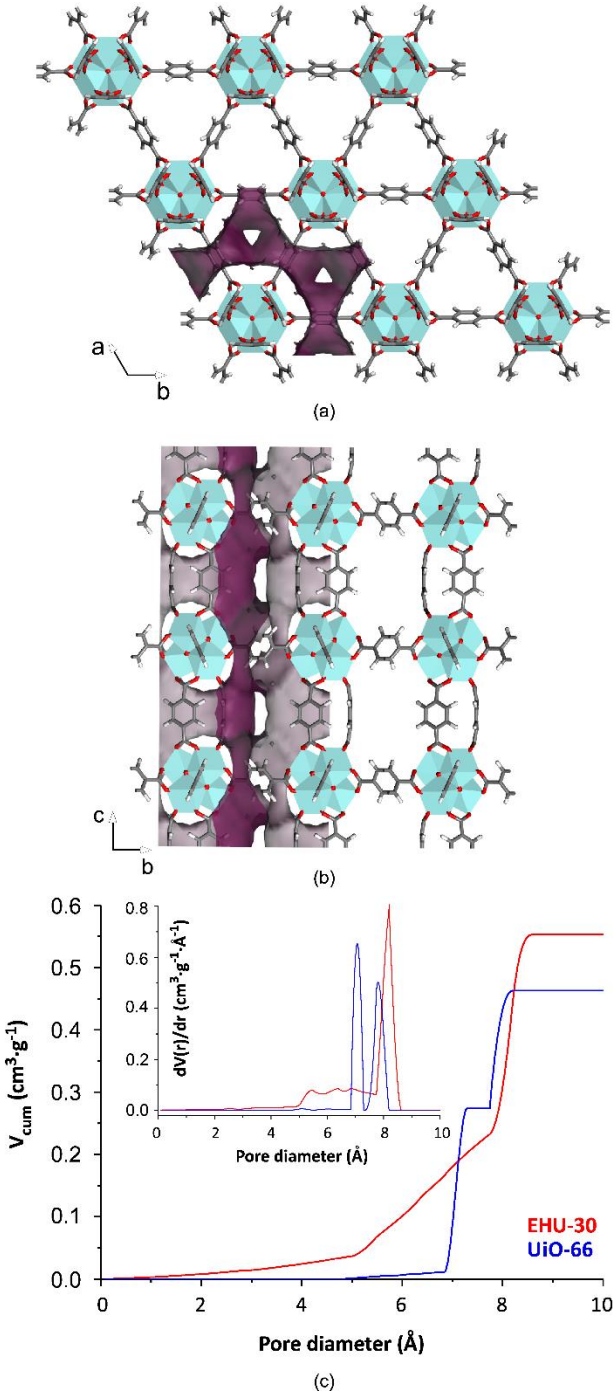

Fig. 2. Crystal packing views of EHU-30 along (a) [001] and (b) [100] crystallographic directions. (c) Pore size distribution analysis depicted as cumulative and derivative (inset) accessible pore volumes.

In order to analyse the differences between the underlying pore networks of EHU-30 and UiO-66, we have computed their geometric pore size distribution (Fig. 2c) by means of a Monte Carlo procedure implemented within a code developed by L. Sarkisov, in which the Lennard-Jones universal force field parameters are used to describe the MOF atoms while the accessible pore volume is assessed by both a gradually

increasing probe and He probe.[22] The results of this analysis show that the prismatic pore cage size of EHU-30 (mode: 8.3 Å) surpasses the mean dimensions of the octahedral and tetrahedral cages (mode: 7.1 and 7.9 Å) of UiO-66. As a result, EHU-30 presents a greater accessible pore volume than UiO-66 (0.534 and 0.428 $cm^3 \cdot g^{-1}$, respectively) resulting into a lighter structure (crystallographic density: 1.10 *vs.* 1.24 $g \cdot cm^{-3}$; porosity: 59 *vs.* 53%).

The permanent porosity of the EHU-30 was further explored by the measurement of nitrogen adsorption isotherm at 77 K. The experimental data were compared with the simulated isotherms for EHU-30 and UiO-66 (Fig. 3) computed by means of Grand Canonical Monte Carlo (GCMC) calculations. As expected, the adsorption curves fit to a type I isotherm with a sharp knee at low relative pressures ($P/P_0 < 0.04$), which is characteristic of crystalline microporous solids. The more obtuse knee in the experimental isotherm, together with its monotonic increase at intermediate pressures and the condensation at high pressures ($P/P_0 > 0.95$) can be attributed to the contribution of the external surface area of the nanosized crystals. In concordance with the crystallographic pore volumes, simulated N_2 uptake capacity of EHU-30 surpasses slightly that of UiO-66 (saturation at: 322 and 295 $cm^3 \cdot g^{-1}$, respectively); fitting of the curves to the BET equation, under the consistency criteria defined by Roquerol et al., yielded surface area values of 1399 and 1283 $m^2 \cdot g^{-1}$, respectively.[23,24] Regarding the experimental isotherm of EHU-30, N_2 uptake value reached immediately after the micropore filling constitutes the 80% of its computed value, while BET fitting led to a surface area value of 1016 $m^2 \cdot g^{-1}$. The lower gas uptake than the expectation is usually ascribed to crystal defects, significant presence of impurities or incomplete pore evacuation. For instance, previous works demonstrated how the presence of modulators in the synthesis promote the formation of linker defects in UiO-66.[25,26] Accordingly, chemical characterization performed upon EHU-30 showed that *ca*. 6% of the BDC linkers are replaced by methacrylate ligands (see ESI), which might explain the aforementioned deviation.

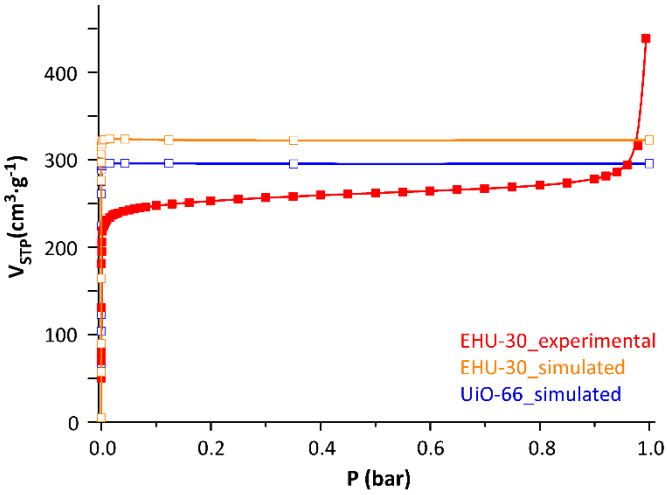

Fig. 3. N_2 (77 K) adsorption isotherms for EHU-30 (experimental and simulation) and UiO-66 (simulation).

Additionally, CO_2 adsorption isotherms were conducted on EHU-30 sample at 298 and 273 K (Fig. S5.2), covering the low pressure range (0–1 bar), in order to estimate isosteric heats of adsorption (Q_{st}) by fitting the data to the modified Clausius–Clapeyron equation.[27,28] The Q_{st} value at zero coverage reaches a value of 28 $kJ \cdot mol^{-1}$ and it decays subtly to a value close to 21 $kJ \cdot mol^{-1}$ at ratio of *ca*. 3 CO_2 molecules per zirconium cluster. These values lie below those reported for most active open-metal sites,[29,30] but agree fairly well with those estimated for UiO-66 (27–24 $kJ \cdot mol^{-1}$).[31]

To get deeper insights into the fundamental differences between both polymorphs, periodic density functional theory (DFT) calculations were used to estimate the relative enthalpic stability. The structures were fully optimized (including atom coordinates and cell parameters) to yield total electronic energies. The more dense-packed UiO-66 is more stable than EHU-30 by 30 $kJ \cdot mol^{-1}$, which suggests a kinetic control upon the isolation of the new polymorph. Accordingly, recent experimental and quantum-chemical calculations on zeolitic imidazolate-frameworks have also evidenced a decrease in energy with increasing density, finding enthalpy differences ranging from 7 to 32 $kJ \cdot mol^{-1}$ within a polymorphic series.[32,33]

At this point, it must be emphasized that the absence of previously reported UiO-66 polymorphs can be related to the strong Zr–O bond and to the resulting rigidity of the SBU/linker ensemble, which apparently hinders template effect to occur. Every framework modification done so far have implied to reduce the linker (BDC) to cluster ratio, so obtained structures cannot be regarded as polymorphs. As aforementioned, the herein employed high reagent concentration enables the methacrylic acid to act both as modulator and structure template. In EHU-30, this template effect, that we believe is based on hydrogen-bonding interactions, implies a distortion of the arrangement of the BDC ligands around the hexanuclear cluster: two triplets of BDC ligands located on opposite triangular faces of the SBU would be forced to get closer by the interacting methacrylic acid (Fig. 4) and therefore they would direct the growth of the crystalline structure in a substantially different way to that taking place in UiO-66. Further evidence of the template effect is inferred from the addition to the reaction of increasing amounts of water, which dilutes the reagents and has the ability to disrupt hydrogen bonding of the template, yielding as a consequence low crystallinity UiO-66 (see ESI).

It deserves to note that according to temperature variable PXRD experiments upon heating EHU-30, non polymorphic phase transition towards thermodynamically favoured phase was observed. Probably because the strength of the zirconium-oxygen bond imposes a too high activation energy barrier for this transition. In fact, EHU-30 exhibits a similar thermal stability to that of UiO-66,[34] being stable up to *ca.* 450 °C after which it decomposes to yield ZrO_2 (see ESI).

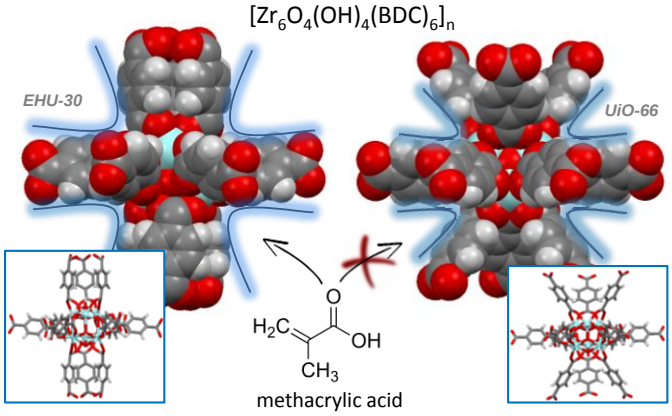

Fig. 4. Detail of the structural differences around the cluster that leads to the formation of EHU-30 and UiO-66.

In summary, this manuscript has introduced the key conditions that lead to the formation of the first reported polymorph of UiO-66, herein named EHU-30. This new polymorph can be regarded as a kinetically favoured metastable structure of $[Zr_6(\mu_3\text{-}O)_4(\mu_3\text{-}OH)_4(\mu_4\text{-}BDC)_6]_n$ that exhibits a rather different topology and surpasses slightly the theoretical porosity of UiO-66. All in all, the herein reported case opens an opportunity to explore the isolation of unprecedented polymorphic series in other group 4 metal MOFs.

This work has been funded by Universidad del País Vasco/Euskal Herriko Unibertsitatea (GIU17/50), Gobierno Vasco/Eusko Jaurlaritza (PIBA18/14) and Ministerio de Economía y Competitividad (MAT2016-75883-C2-1-P). Technical and human support provided by SGIker (UPV/EHU, MICINN, GV/EJ, ESF) is also acknowledged. We thank the Diamond Light Source Ltd for the award of beam time on I11 (allocation EE17788).

Conflicts of interest

There are no conflicts to declare.

Notes and references

‡ Crystallographic data. Crystal system: hexagonal; space group: $P6_3/mmc$; cell parameters: a = 14.6690(4) Å, c = 26.8478(19) Å, V = 5003.1(5) Å^3.

1 H. Furukawa, K. E. Cordova, M. O'Keeffe and O. M. Yaghi, *Science*, 2013, **341**, 1230444.
2 A. Kirchon, L. Feng, H. F. Drake, E. A. Joseph and H.-C. Zhou, *Chem. Soc. Rev.,* 2018, **47**, 8611.
3 C. R. Groom, I. J. Bruno and M. P. Lightfoot, S. C. Ward, *Acta Cryst.*, 2016, **B72**, 171.
4 P. Z. Moghadam, A. Li, S. B. Wiggin, A. Tao, A. G. P. Maloney, P. A. Wood, S. C. Ward and D. Fairen-Jimenez, *Chem. Mater.*, 2017, **29**, 2618.
5 K. S. Park, Z. Ni, A. P. Côte, J. Y. Choi, R. Huang, F. J. Uribe-Romo, H. K. Chae, M. O'Keeffe and O. M. Yaghi, *PNAS*, 2006, **103**, 10186.
6 T. Devic and C. Serre, *Chem. Soc. Rev.*, 2014, **43**, 6097.
7 S. Yuan, J.-S. Qin, C. T. Lollar and H.-C. Zhou, *ACS Cent. Sci.*, 2018, **4**, 440.
8 J. H. Cavka, S. Jakobsen, U. Olsbye, N. Guillou, C. Lamberti, S. Bordiga and K. P. Lillerud, *J. Am. Chem. Soc.*, 2008, **130**, 13850.
9 S. Waitschat, H. Reinscha and N. Stock, *Chem. Commun.*, 2016, **52**, 12698.
10 S. Yuan, W. Lu, Y.-P. Chen, Q. Zhang, T.-F. Liu, D. Feng, X. Wang, J. Qin and H.-C. Zhou, *J. Am. Chem. Soc.*, 2015, **137**, 3177.
11 V. Bon, I. Senkovska, I. A. Baburin and S. Kaskel, *Cryst. Growth Des.*, 2013, **13**, 1231.
12 D. Feng, Z.-Y. Gu, J.-R. Li, H.-L. Jiang, Z. Wei and H.-C. Zhou, *Angew. Chem. Int. Ed.*, 2012, **51**, 10307.
13 D. Feng, W.-C. Chung, Z. Wei, Z.-Y. Gu, H.-L. Jiang, Y.-P. Chen, D. J. Darensbourg and H.-C. Zhou, *J. Am. Chem. Soc.*, 2013, **135**, 17105.
14 V. Bon, I. Senkovska, M. S. Weiss and S. Kaskel, *CrystEngComm*, 2013, **15**, 9572.
15 H. Furukawa, F. Gándara, Y.-B. Zhang, J. Jiang, W. L. Queen, M. R. Hudson and O. M. Yaghi, *J. Am. Chem. Soc.*, 2014, **136**, 4369.
16 Y. Bai, Y. Dou, L.-H. Xie, W. Rutledge, J.-R. Li and H.-C. Zhou, *Chem. Soc. Rev.*, 2016, **45**, 2327.
17 G. Liu, Z. Ju, D. Yuan and M. Hong, *Inorg. Chem.*, 2013, **52**, 13815.
18 V. Guillerm, S. Gross, C. Serre, T. Devic, M. Bauer and G. Férey, *Chem. Commun.*, 2010, **46**, 767.
19 Topos Main Page http://www.topospro.com (accessed: 2019/01/23).
20 V. A. Blatov, A. P. Shevchenko and D. M. Proserpio, *Cryst. Growth Des.*, 2014, **14**, 3576.
21 L. H. T. Nguyen, T. T. Nguyen, H. L. Nguyen, T. L. H. Doan and P. H. Tran, *Cat. Sci. Tech.*, 2017, **7**, 4346.
22 L. Sarkisov, *Molecular Simulation*, 2011, **37**, 1248.
23 S. Brunauer, P. H. Emmett and E. J. Teller, *J. Am. Chem. Soc.,* 1938, **60**, 309.
24 J. Rouquerol, P. Llewellyn and F. Rouquerol, *Stud. Surf. Sci. Catal.*, 2007, **160**, 49.
25 G. C. Shearer, S. Chavan, S. Bordiga, S. Svelle, U. Olsbye and K. P. Lillerud, *Chem. Mater.*, 2016, **28**, 3749.
26 M. J. Katz, Z. J. Brown, Y. J. Colón, P. W. Siu, K. A. Scheidt, R. Q. Snurr, J. T. Hupp and O. K. Farha, *Chem. Commun.*, 2013, **49**, 9449.
27 K. Sumida, D. L. Rogow, J. A. Mason, T. M. McDonald, E. D. Bloch, Z. R. Herm, T.-H. Bae and J. R. Long, *Chem. Rev.*, 2012, **112**, 724.
28 H. Pan, J. A. Ritter and P. B. Balbuena, *Langmuir*, 1998, **14**, 6323.
29 M. Fischer, J. R. B. Gomes and M. Jorge, *Molecular Simulation*, 2014, **40**, 537.
30 S. Nandi, P. De Lujna, R. D. Daff, J. Rother, M. Liu, W. Buchanan, A. I. Hawari, T. K. Woo and R. Vaidhyanathan, *Sci. Adv.*, 2015, **1**, e1500421.
31 G. E. Cmarik, M. Kim, S. M. Cohen and K. S. Walton, *Langmuir*, 2012, **28**, 15606.
32 Q. Shi, W.-J. Xu, R.-K. Huang, W.-X. Zhang, Y. Li, P. Wang, F.-N. Shi, L. Li, J. Li and J. Dong, *J. Am. Chem. Soc.*, 2017, **139**, 7952.
33 A. Shrotri, H. Kobayashi and A. Fukuoka, *Acc. Chem. Res.*, 2018, **51**, 659.
34 L. Valenzano, B. Civalleri, S. Chavan, S. Bordiga, M. H. Nilsen, S. Jakobsen, K. P. Lillerud and C. Lamberti, *Chem. Mater.*, 2011, **23**, 1700.